Volume 59
Number 19
7 March 2023
Pages 2671–2830

ChemComm

Chemical Communications

rsc.li/chemcomm

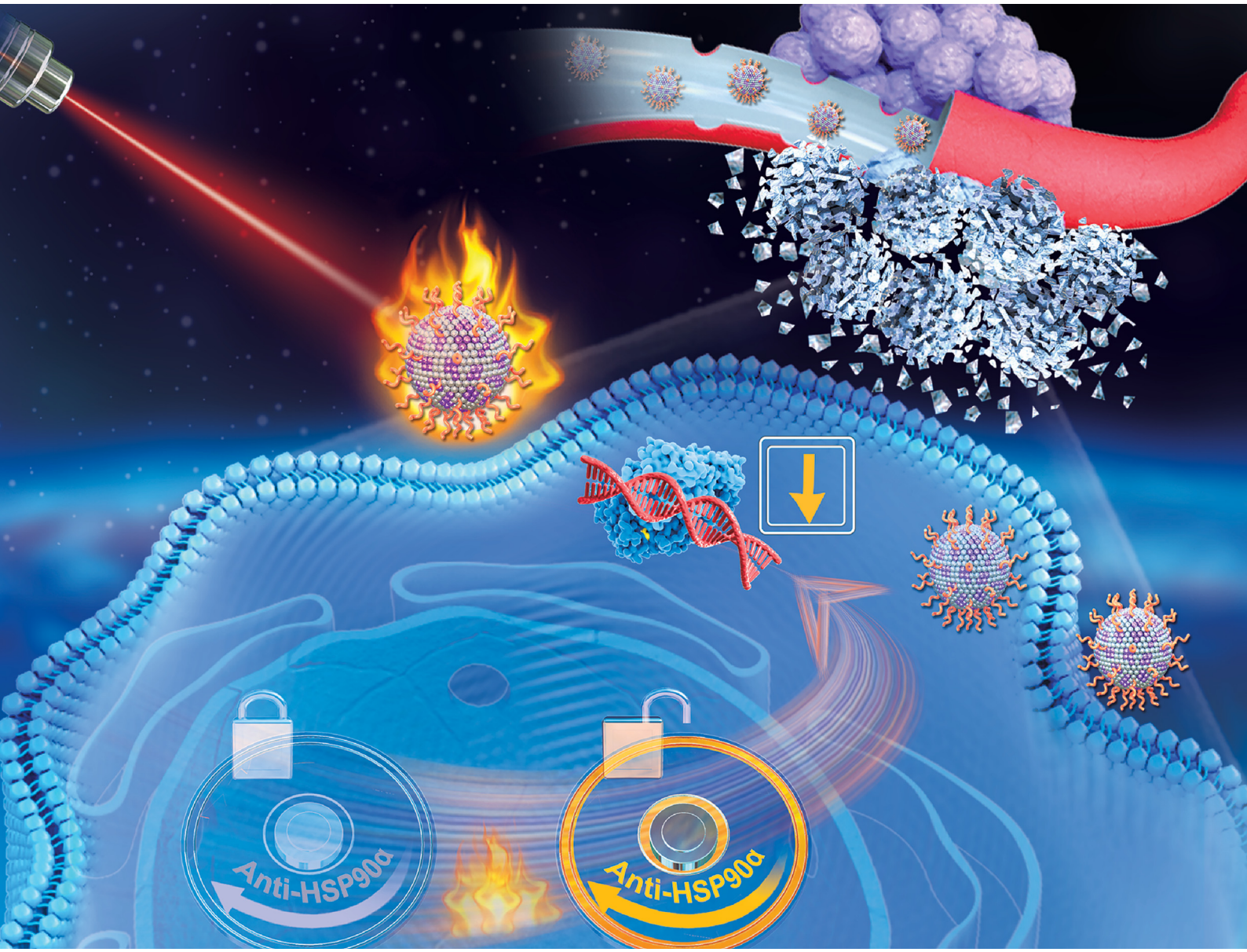

ISSN 1359-7345

ROYAL SOCIETY OF CHEMISTRY

COMMUNICATION

Rong Hu, Anjun Qin, Ben Zhong Tang *et al.*
NIR luminogen for low-temperature photothermal therapy by triggering HSP90α down-regulation

ChemComm

COMMUNICATION

View Article Online
View Journal | View Issue

Cite this: *Chem. Commun.*, 2023, 59, 2743

Received 20th December 2022,
Accepted 27th January 2023

DOI: 10.1039/d2cc06932f

rsc.li/chemcomm

NIR luminogen for low-temperature photothermal therapy by triggering HSP90α down-regulation†

Xinzhe Yang,‡[ab] Keke Ding,‡[f] Guiquan Zhang,[ab] Pengbo Han,[ab] Rong Hu,*[abe] Zhiming Wang,[ab] Anjun Qin*[ab] and Ben Zhong Tang*[bcd]

A near-infrared (NIR) luminogen TST was designed and used to efficiently trigger HSP90α protein knockdown through photothermal conversion based on a gene interference strategy, by which *in vitro* and *in vivo* tumor ablation were significantly acquired at low-temperature.

As a growing global threat, cancer has developed as a leading cause of death.[1] The traditional treatments are still the primary clinical approaches for cancer therapy; however, the high dependence on professional proficiency and the severe sequelae should be conquered.[2] A variety of therapeutic strategies have been developed to meet the demands of desirable accuracy and low side-effects.[3] Photothermal therapy (PTT) has been developed as a promising approach for cancer therapy thanks to its remarkable capacity of light-controllable and non-invasive modalities.[3,4] However, excessive heat with uncontrollable diffusion will pose a threat to surrounding tissues, and further develop thermal resistance and trigger inflammatory storms.[5] Detailed studies have shown that heat resistance is related to the over-expression of heat shock proteins (HSPs),[6] and HSP90 is overexpressed in tumor cells to maintain homeostasis in harsh microenvironments and promote cell survival in stressed environments, reducing the treatment efficacy of PTT.[7]

The development of low-temperature PTT could effectively inhibit the heat resistance of tumors with high treatment efficiency.[8] However, the therapeutic effect of low-temperature PTT alone is limited owing to the decreased temperature. Thus, multiple treatment modalities were used to achieve better treatment effects. Recently, the realization of adjuvant therapy for cancer based on gene interference has become a hot research topic by regulating the expression of disease-related biomacromolecules.[9] By reducing the HSP90α level, the sensitivity of tumor cells towards heat can be efficiently enhanced and this can improve the therapeutic effect of PTT.[8] The combination of gene interference and PTT in tumor therapy is expected to improve the therapeutic efficiency with a desirable effect.

It is well-known that near-infrared (NIR) light possesses deeper tissue penetration and minimal light damage to biological systems.[10] Various NIR luminogens, including quantum dots, organic fluorophores and conjugated polymers, have been prepared for tumor imaging and therapy.[4,11] In particular, organic NIR luminogens with aggregation-induced emission (AIE) features possess outstanding optical properties, good biosafety and perfect processability, which could utilize aggregation to enhance their emission, making them ideal candidates for *in vivo* tracing and tumor diagnosis.[12] Moreover, these luminogens always present efficient photo-thermal transformation, showing high promise for tumor therapy-based PTT.

Herein, by combination of PTT and gene interference, a NIR luminogen of TST was rationally designed and synthesized, which could trigger the down-regulation of HSP90α in a thermal-responsive way, and further realize the low-temperature PTT of tumors *in vitro* and *in vivo*. As illustrated in Fig. 1, TST nanoparticles (NPs) with NIR emission and efficient photo-thermal conversion could be facilely constructed by using DSPE-PEG2000 as the matrix. Before the NP treatment, tumor cells were transfected with HSP90α siRNA by retrovirus infection, which could be

[a] *State Key Laboratory of Luminescent Materials and Devices, Guangdong Provincial Key Laboratory of Luminescence from Molecular Aggregates, South China University of Technology, Guangzhou, 510640, China. E-mail: msqinaj@scut.edu.cn, hurong@usc.edu.cn*

[b] *Center for Aggregation-Induced Emission, AIE Institute, South China University of Technology, Guangzhou, 510640, China*

[c] *School of Science and Engineering, Shenzhen Institute of Aggregate Science and Technology, The Chinese University of Hong Kong, Shenzhen, Guangdong, 518172, China. E-mail: tangbenz@cuhk.edu.cn*

[d] *Hong Kong Branch of Chinese National Engineering Research Centre for Tissue Restoration and Reconstruction, The Hong Kong University of Science & Technology, Clear Water Bay, Kowloon, Hong Kong, China*

[e] *School of Chemistry and Chemical Engineering, University of South China, Hengyang, 421001, China*

[f] *Department of Urology, The First Affiliated Hospital of Soochow University, NO. 188 Shizi Road, Suzhou, 215006, China*

† Electronic supplementary information (ESI) available: Experimental details, and structural characterization of TST, and the bio-applications of TST-based nanoparticles. See DOI: https://doi.org/10.1039/d2cc06932f

‡ These authors contributed equally to this work.

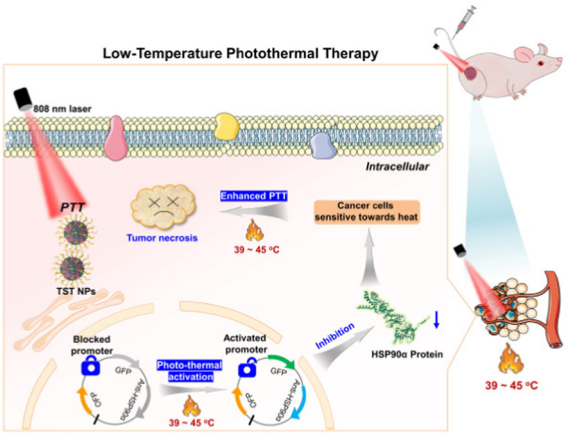

Fig. 1 Schematic illustration of low-temperature photothermal therapy based on TST by triggering HSP90α down-regulation.

activated upon heating ($\geq$39 °C) to reduce the expression of HSP90α. Upon 808 nm laser irradiation, the sensitivity of tumor cells towards heat was efficiently improved with the knockdown of HSP90α. As a result, effective tumor ablation could be acquired at low temperature without excessive damage towards normal tissues.

The synthetic route to TST (4,8-bis(5-(4-(bis(4-methoxyphenyl) amino)phenyl)-4-(2-ethylhexyl)thiophen-2-yl)benzo[1,2-*c*:4,5*c*′]bis[1,2,5]thiadiazole) is shown in Fig. 2A. The Suzuki coupling of dibromo-compound **1** with strong electron-withdrawing ability and the electron-donating triphenylamine containing boronic acid **2** readily produced the target molecule TST (Fig. S1–S3, ESI†). The photophysical property measurement revealed that TST showed a maximum absorption at 850 nm and emission peaks at 1125 nm and *ca.* 1230 nm in THF (Fig. 2B). The shoulder emission might suggest that

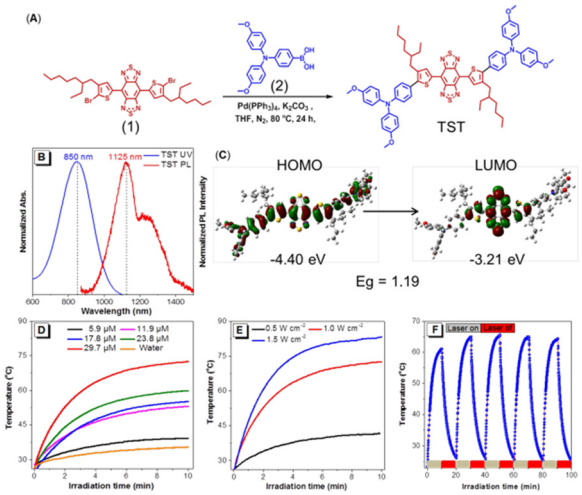

Fig. 2 (A) Synthetic route to TST. (B) Normalized absorption and photoluminescence spectra of TST in THF. Concentration of TST: 10 μM; λ_{ex}: 850 nm. (C) HOMO and LUMO distribution and the energy states of TST. (D) and (E) Heating curves of TST NPs with different concentration and laser power, respectively. (F) Photothermal stability of TST NPs under 808 nm laser (1 W cm^{-2} for 10 min) irradiation with five heating/cooling cycles.

there exist intermolecular interactions besides the twisted intramolecular charge transfer (TICT) effect. Moreover, its emission located in the range of the NIR II region, which is beneficial for *in vivo* imaging with deep penetration ability and promising for PTT applications. The fluorescence quantum yield of TST in THF solution was measured to be 0.6%, and the related NPs in PBS were 1.5%, indicative of its AIE feature. In addition, the theoretical calculation results (Fig. 2C) based on density functional theory (DFT) at the M06-2X/6-31G(d,p) level indicated that the band gap (E_g) of TST was 1.19 eV, and the lowest unoccupied molecular orbital (LUMO) and the highest molecular orbital (HOMO) were calculated to be −3.21 eV and −4.40 eV, respectively. The presence of strong electron-donating methoxyl groups readily promotes the intramolecular charge transfer (ICT) process and reduces the band gap, enhancing the vibration coupling between the ground state and the excited state of TST. To enhance the solubility and biocompatibility of TST for bio-applications, DSPE-PEG2000 was employed as the matrix to construct TST NPs (Fig. S4A and B, ESI†). The particle size of the TST NPs measured by dynamic light scattering (DLS) and transmission electron microscopy (TEM) was 134 nm and 78 nm, respectively (Fig. S4C and D, ESI†), and the zeta potential of the TST NPs was −36.7 mV, which facilitates their biomedical applications.

Next, the photo-thermal behavior of the TST NPs was studied. As expected, the temperature increment distribution at 808 nm laser exposure exhibited significant concentration and laser power dependence (Fig. 2D and E), which suggests that the desired temperature could be well fine-tuned. It is worth noting that TST NPs showed excellent stability of photothermal conversion with efficiency of 22.6%. As shown in Fig. 2F, after five cycles of heating and cooling, the maximum value could still be recovered and the temperature was close to the original level (61.5 °C). Moreover, the TST NPs presented excellent thermal imaging ability in water upon laser irradiation (Fig. S5, ESI†).

After investigating the photophysical and photothermal properties of TST, the thermal-sensitive behavior of transfected cells was studied. The representative cell lines, MCF-7 and A549, were transfected with the designed exogenous gene. According to our design principle, after successful transfection, bright orange fluorescence could be detected inside cells because of the expression of orange fluorescent protein (OFP). Furthermore, the HSP90α resistance gene could be promoted *via* heat activation ($\geq$39 °C) with the expression of green fluorescence protein (GFP), which could be realized by precisely regulating the temperature based on the photothermal conversion of TST NPs. Subsequently, the HSP90α resistance gene was expressed with the synthesis of the related siRNA to prevent the translation of HSP90α, resulting in their decreased expression and the reduced heat tolerance of tumor cells. The successful transfection of the designed exogenous gene was verified because a bright orange fluorescence could be detected inside the aforementioned cell lines (Table S1, ESI†). By systematically optimizing the effect of temperature and time on the triggering of HSP90α down-regulation, temperatures in the range of 42 to 45 °C with the duration time of 10 min could realize the activation of the HSP90α resistance gene (Tables S2 and S3, ESI†).

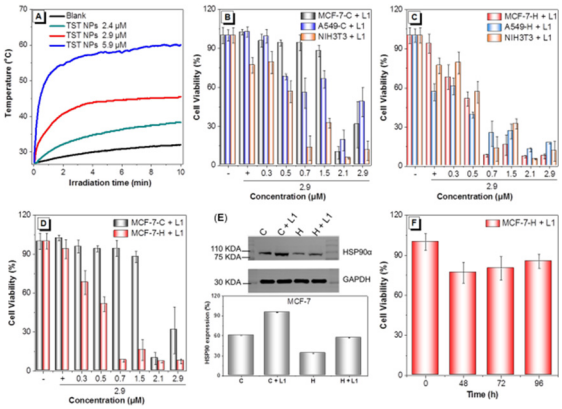

Fig. 3 (A) Heating curves of TST NPs in culture medium under an 808 nm laser with different concentrations. (B) Cell viability of the control group and (C) HSP90α knockdown cells treated with TST NPs with one light irradiation. (D) Cell viability of MCF-7-C and MCF-7-H cells treated with TST NPs with one light irradiation. (E) WB analysis of the HSP90α expression in MCF-7-C and MCF-7-H cells treated by TST NPs (2.9 μM) with or without 808 nm laser irradiation. (F) Cell viability of MCF-7-H cells treated with TST NPs with one light irradiation, followed by different incubation times (808 nm laser irradiation, 1 W cm^{-2} for 10 min, [TST NPs] = 2.9 μM).

To optimize the desirable temperature based on TST NPs, the temperature variation of TST NPs with different concentrations was recorded. As shown in Fig. 3A, the temperature could be stabilized at 44 °C with 2.9 μM of TST NPs for 10 min upon 808 nm laser irradiation, which was set as the following experimental conditions. To evaluate the role of HSP90α in heat tolerance, the cell viabilities in control groups without HSP90α resistance gene transfection (MCF-7-C and A549-C) and HSP90α knockdown groups (MCF-7-H and A549-H) were investigated and compared. And the results revealed that the viability of tumor cells of MCF-7-C and A549-C was slightly higher than that of normal ones (NIH 3T3) in the control group (Fig. 3B). It is worth noting that the cell survival rate remarkably increased at high concentrations of TST NPs, which might be due to the overexpression of HSP90α under elevated temperature. Meanwhile, in the HSP90α knockdown groups (MCF-7-H and A549-H), the survival rate of tumor cells was lower than that of normal cells (NIH 3T3) (Fig. 3C). These results indicated that the knockdown of HSP90α made the tumor cells more sensitive towards heat than that of normal cells, laying a good foundation for low-temperature PTT. In addition, the comparison of the MCF-7-C and MCF-7-H cell survival rates further demonstrated that the knockdown of HSP90α reduced the cell thermal tolerance and increased the sensitivity to PTT (Fig. 3D).

To evaluate the thermal initiation of HSP90α down-regulation by TST NPs, the expression of GFP inside transfected cells was displayed by fluorescence imaging. A bright green fluorescence could be observed in MCF-7-H and A549-H treated with TST NPs (2.9 μM) under 808 laser irradiation (Tables S4 and S5, ESI†), indicative of the successful triggering of HSP90α resistance gene expression. A Western Blot (WB) was employed to verify the initiation. As shown in Fig. 3E and Fig. S6B (ESI†), the results revealed that the expression level of HSP90α in MCF-7-H and A549-H was significantly decreased compared with that of the control groups. Moreover, the cell viability of MCF-7-H showed that the survival rate remained unchanged, indicating that the knockdown of HSP90α would inhibit the proliferation of cells (Fig. 3F). Thus, for MCF-7-H cells, the efficient inhibition of tumor cells was realized with TST NP treatment based on one laser irradiation, because the down-regulation of HSP90α has an obvious effect on tumor proliferation. Meanwhile, for the control groups, twice laser irradiation was needed for tumor cell ablation (Fig. S7, ESI†). A549 cells also showed a similar survival trend, indicative of the universality of this strategy to tumor cells (Fig. S6A, ESI†). Thus, based on the down-regulation of HSP90α activated by the TST NP photo-thermal effect, efficient tumor inhibition *via* low-temperature PTT was realized at the cellular level successfully.

Afterwards, the *in vivo* evaluation of the treatment effect *via* low-temperature PTT was conducted on an MCF-7-H-skin-tumor-bearing BALB/c Nude mouse model. The experiment process was illustrated in Fig. 4A. First, the *in vivo* distribution of TST NPs after intravenous injection was studied. As shown in Fig. 4B, thermal imaging analysis revealed that tumor tissues could reach 44 °C under 808 nm laser irradiation with the treatment of TST NPs. Meanwhile, for the blank groups, the related temperature was recorded to be 37 °C under the same conditions, indicating the successful enrichment of TST NPs in the tumor tissue. Moreover, the fluorescence of TST NPs could be detected after 96 h by *in vivo* fluorescent imaging (Fig. S8, ESI†), indicative of the good retention ability and outstanding

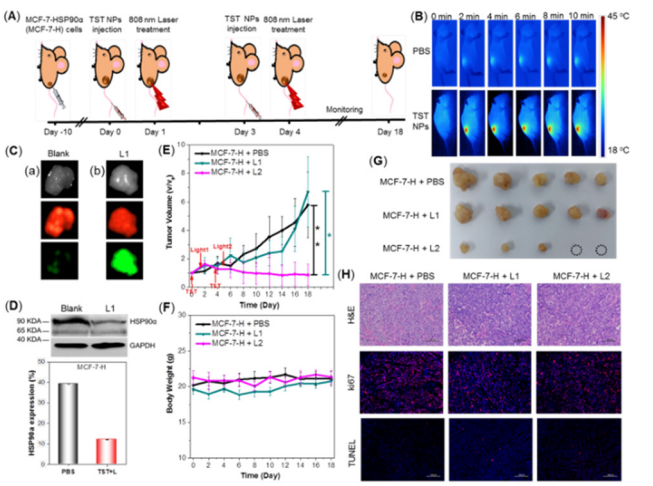

Fig. 4 (A) Schematic illustration of tumor growth and treatment in mice. (B) NIR thermal images of tumors in mice with or without intravenous injection of TST NPs after 24 h under laser irradiation. (C) Fluorescence imaging of MCF-7-H-bearing mice treated with PBS (a) or TST NPs with laser irradiation (b) after 48 h. (D) WB analysis of HSP90α expression in MCF-7-H tumors with different treatments. (E) Growth curves of tumors in mice (n = 5) after treatment by PBS, and TST NPs with once or twice irradiation. (F) Body weight curves of MCF-7-H tumor-bearing mice after different treatments. (G) Representative tumor images of MCF-7-H-bearing mice for 18 days after different treatments. (H) H&E, Ki67 (red fluorescence), and TUNEL (red fluorescence) staining of tumor tissues with different treatments.

tracing behavior of tumor tissue. The expression of OFP and GFP in the tumor tissue was investigated to figure out the construction of a mouse model by transfected cells and the expression of the HSP90α resistance gene *in vivo*. As shown in Fig. 4C, both bright orange and green fluorescence could be detected inside the tumor tissue in the TST NP-treated groups upon light irradiation, verifying the successful transfection and initiation of the HSP90α resistance gene *in vivo*. Moreover, the expression of HSP90α protein in tumor tissue was also significantly reduced in the light irradiation groups compared with the blank ones (Fig. 4D).

After confirming the successful enrichment of NPs in the tumor tissues and triggering HSP90α knockdown, the tumor inhibition behavior was investigated. The mice were randomly divided into the following three groups: blank groups (MCF-7-H + PBS), MCF-7-H bearing mice with TST NP treatment followed by one laser irradiation (MCF-7-H + L1) and two laser irradiations (MCF-7-H + L2). As shown in Fig. 4E, after the intravenous injection of TST NPs with one laser irradiation, the growth of the tumors was only inhibited slightly compared with the blank groups, which meant that the trigger of HSP90α knockdown couldn't efficiently inhibit tumors *in vivo*. Meanwhile, for the group with twice laser irradiation to proceed low-temperature PTT, the tumor was significantly inhibited and a trend of ablation could be observed (Fig. 4G and Fig. S9, ESI†). The antitumor efficiency was also verified by the hematoxylin and eosin (H&E) and immunofluorescent staining of tumor tissues with different treatments. As shown in Fig. 4H, H&E staining results demonstrated that tumors with both once and twice laser irradiation presented necrosis and fragmentation of the tumor cells. And the expression of Ki67, related to mitosis, was obviously reduced in these two groups compared with the blank one. Meanwhile, there was no significant difference in TUNEL staining among these groups. These results presented that the tumor cells were ablated through the necrosis process to realize tumor inhibition based on PTT at low temperature. Meanwhile, both TST NP treatment and laser irradiation presented a negligible effect on body weight (Fig. 4F). Furthermore, hemolysis experiments revealed that no hemolysis was observed for blood treated with TST NPs (Fig. S10, ESI†). The functional biomarkers of the liver and kidneys were evaluated as well, and no differences among these groups were detected (Fig. S11, ESI†). The outstanding biosafety of the TST NPs was also proved by the H&E staining of organs with different treatments (Fig. S12, ESI†). Combining these results, the TST NPs showed high promise for tumor treatment through low temperature PTT with high efficiency and good biosafety.

An efficient low temperature PTT approach based on NIR luminogen TST with desirable photothermal conversion was realized in this work. By pre-transfection with HSP90α silencing gene, the heat tolerance of tumor cells would be efficiently inhibited by reducing the expression of HSP90α in a thermal-responsive way. Upon laser irradiation, the sensitivity of the tumor cells towards heat was drastically improved after treatment with TST NPs. Thus, *in vitro* and *in vivo* tumor inhibition at low temperature was achieved efficiently without any damage to the surrounding normal tissues. This work presents an excellent strategy of NIR organic materials for low-temperature PTT of tumors in the clinic.

X. Y., K. D., and R. H. conceived the experiments. X. Y. was responsible for all the experiments. K. D. was responsible for antitumor experiments *in vivo*. P. H., G. Z., R. H., A. Q., and B. Z. T. provided the suggestions in the experimental process. X. Y., K. D., G. Z., P. H., R. H., Z. W., A. Q., and B. Z. T. contributed to the writing of this paper.

This work was financially supported by the National Natural Science Foundation of China (21788102 and 21907034), the Natural Science Foundation of Guangdong Province (2019B030301003), the National Key Research and Development Program of China (Intergovernmental cooperation project, 2017YFE0132200) and the Innovation and Technology Commission of Hong Kong (ITC-CNERC14S01).

Conflicts of interest

There are no conflicts to declare.

Notes and references

1 (*a*) D. Hanahan and R. A. Weinberg, *Cell*, 2000, **100**, 57–70; (*b*) D. W. Felsher, *Nat. Rev. Cancer*, 2003, **3**, 375–380.
2 J. Wang, X. Wang, K. Yang, S. Hu and W. Wang, *Biosensors*, 2022, **12**, 683.
3 J. Huang, B. He, Z. Zhang, Y. Li, M. Kang, Y. Wang, K. Li, D. Wang and B. Z. Tang, *Adv. Mater.*, 2020, **32**, 2003382.
4 Y. Liu, P. Bhattarai, Z. Dai and X. Chen, *Chem. Soc. Rev.*, 2019, **48**, 2053.
5 G. Gao, Y. W. Jiang, W. Sun, Y. Guo, H. R. Jia, X. W. Yu, G. Y. Pan and F. G. Wu, *Small*, 2019, **15**, e1900501.
6 G. Gao, X. Sun and G. Liang, *Adv. Funct. Mater.*, 2021, **31**, 2100738.
7 (*a*) L. Whitesell and S. L. Lindquist, *Nat. Rev. Cancer*, 2005, **5**, 761–772; (*b*) G. Zhang, W. Cheng, L. Du, C. Xu and J. Li, *J. Nanobiotechnol.*, 2021, **19**, 9.
8 (*a*) X. Li, Y. Pan, C. Chen, Y. Gao, X. Liu, K. Yang, X. Luan, D. Zhou, F. Zeng, X. Han and Y. Song, *Angew. Chem., Int. Ed.*, 2021, **60**, 21200–21204; (*b*) G.-F. Luo, J.-L. Liang, D.-W. Zheng, P. Ji, J.-W. Wang, W.-H. Chen and X.-Z. Zhang, *Adv. Funct. Mater.*, 2022, **32**, 2205550.
9 (*a*) Y. Cheng, C. Sun, R. Liu, J. Yang, J. Dai, T. Zhai, X. Lou and F. Xia, *Angew. Chem., Int. Ed.*, 2019, **58**, 5049–5053; (*b*) M. Matsui and D. R. Corey, *Nat. Rev. Drug Discovery*, 2017, **16**, 167–179.
10 (*a*) C. Yang, W. Zhang, X. Pang, F. Xiao, S. Kumar Kalva, Y. Zhang, M. Pramanik, L. Tian, G. Liu and M. Wang, *Aggregate*, DOI: 10.1002/agt2.261; (*b*) Y.-F. Xiao, F.-F. An, J.-X. Chen, J. Yu, W.-W. Tao, Z. Yu, R. Ting, C.-S. Lee and X.-H. Zhang, *Small*, 2019, **15**, 1903121.
11 B. Huang, X. Liu, G. Yang, J. Tian, Z. Liu, Y. Zhu, X. Li, G. Yin, W. Zheng, L. Xu and W. Zhang, *CCS Chem.*, 2022, **4**, 2090–2101.
12 G. Feng, G.-Q. Zhang and D. Ding, *Chem. Soc. Rev.*, 2020, **49**, 8179.

